Annual Report
Hydrospheric Atmospheric Research Center (HyARC)
Nagoya University

2011

Contents

Foreword

On March 11, 2012, a catastrophic earthquake occurred off the coast of Japan. The disastrous earthquake affected us throughout the 2012 fiscal year. Although, the impact of the earthquake on the Hydrospheric Atmospheric Research Center (HyARC) was limited, the earthquake forced us to think deeply about the relationship between science and society. The results of scientific research do not always give us a direct benefit, but a prompt response to direct disasters is strongly expected by our society. Scientific research is supported by society, and we cannot ignore its possible contribution to society.

The research environment is changing and becoming more competitive. The competition is not only for the research budget but also for the researchers themselves. Even capable researchers are leaving the research community, and those working at HyARC are no exception.

As described in this annual report, the research activity at HyARC is maintained at a high level and the themes of the studies are diverged. Since it is natural that the researche field diverges as their research progresses, this divergence should be acknowledged. However, HyARC has its own research objective, that is, investigating the mechanism of the global water cycle, and we should always be careful to coordinate between individual research and HyARC's objective.

HyARC functions as an inter-university collaborative system, which is in many ways unique in the world. To ensure its research activity, HyARC was accredited as a Joint Usage/Research Center in April 2010 by the Ministry of Education, Culture, Sports, Science, and Technology, Japan.

The University Project supported a virtual laboratory for diagnosing the earth's climate system.

HyARC has also collaborated with numerous institutions such as the Research Institute of Humanity and Nature (RIHN) and the National Institute of Information and Communication Technology (NICT). HyARC has also taken part in international collaborations. As part of the UNESCO International Hydrology Program (IHP), HyARC has hosted training courses supported by the Japan Trust Fund. This year's course was conducted by the Disaster Prevention Research Institute, Kyoto University. While selecting projects and activities, HyARC considers the project's feasibility, its significance, and the collaboration requirements. Although HyARC has only 10 permanent staff members (four professors, three associate professors, and three assistant professors), it supports many postdoctoral candidates in active research. In addition, HyARC has accepted graduate students in the Department of Environmental Studies.

Nakamura Kenji
Director
Hydrospheric Atmospheric Research Center

Staff and Organization

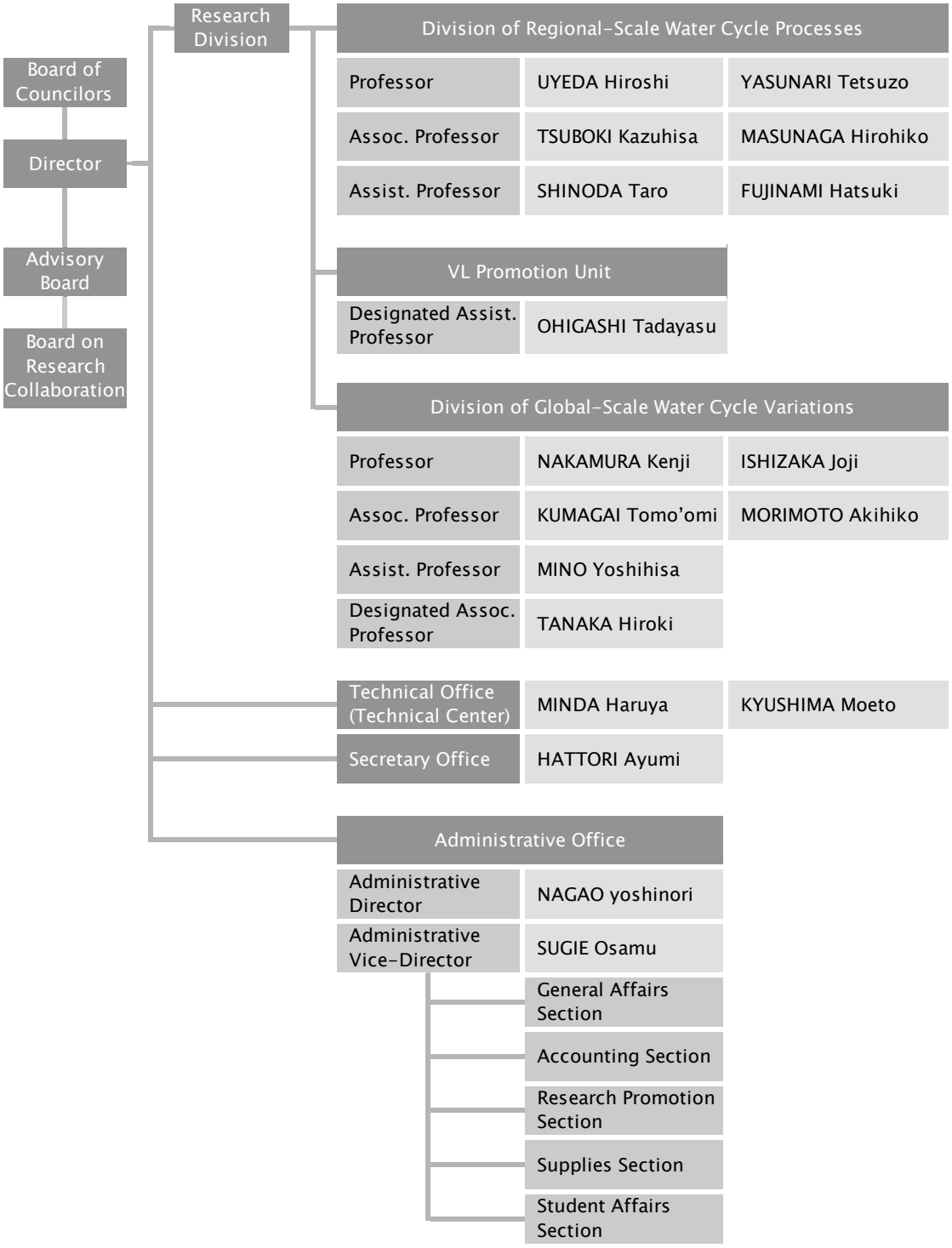

Administration

Board of Councilors

NAKAMURA Kenji: Director, Prof., Hydrospheric Atmospheric Research Center, Nagoya University
UYEDA Hiroshi: Prof., Hydrospheric Atmospheric Research Center, Nagoya University
YASUNARI Tetsuzo: Prof., Hydrospheric Atmospheric Research Center, Nagoya University
ISHIZAKA Joji: Prof., Hydrospheric Atmospheric Research Center, Nagoya University
TANAKA Kentaro: Prof., Graduate School of Science, Nagoya University
TSUJIMOTO Tetsuro: Prof., Graduate School of Engineering, Nagoya University
TAKENAKA Chisato: Prof., Graduate School of Bioagricultural Sciences, Nagoya University
KANZAWA Hiroshi: Prof., Graduate School of Environmental Studies, Nagoya University
MATSUMI Yutaka: Prof., Solar-Terrestrial Environment Laboratory, Nagoya University

Advisory Board

●Members from Nagoya University

UYEDA Hiroshi: Prof., Hydrospheric Atmospheric Research Center, Nagoya University
YASUNARI Tetsuzo: Prof., Hydrospheric Atmospheric Research Center, Nagoya University
ISHIZAKA Joji: Prof., Hydrospheric Atmospheric Research Center, Nagoya University
TSUBOKI Kazuhisa: Assoc. Prof., Hydrospheric Atmospheric Research Center, Nagoya University
MASUNAGA Hirohiko: Assoc. Prof., Hydrospheric Atmospheric Research Center, Nagoya University
KUMAGAI Tomo'omi: Assoc. Prof., Hydrospheric Atmospheric Research Center, Nagoya University
MORIMOTO Akihiko: Assoc. Prof., Hydrospheric Atmospheric Research Center, Nagoya University

●Members outside Nagoya University

FUJIYOSHI Yasushi: Prof., Institute of Low Temperature Science, Hokkaido University
HANAWA Kimio: Prof., Graduate School of Science, Tohoku University
SUMI Akimasa: Prof., Integrated Research System for Sustainability Science, The University of Tokyo
FUKUSHIMA Yoshihiro: Designated Prof., Tottori University of Environmental Studies
YAMANAKA Manabu: Principal Scientist, Research Institute for Global Change, Japan Agency for Marine-Earth Science and Technology
YAMANOUCHI Takashi: Prof., National Institute of Polar Research
TANIGUCHI Makoto: Prof., Research Institute for Humanityand Nature
OKI Riko: Senior Researcher, Earth Observation Research Center, Japan Aerospace Exploration Agency

Board on Research Collaboration

●Members from Nagoya University

UYEDA Hiroshi: Prof., Hydrospheric Atmospheric Research Center, Nagoya University
ISHIZAKA Joji: Prof., Hydrospheric Atmospheric Research Center, Nagoya University
MORIMOTO Akihiko: Assoc. Prof., Hydrospheric Atmospheric Research Center, Nagoya University

●Members outside Nagoya University

FUJIYOSHI Yasushi: Prof., Institute of Low Temperature Science, Hokkaido University
YAMANAKA Manabu: Principal Scientist, Research Institute for Global Change, Japan Agency for Marine-Earth Science and Technology
TANIGUCHI Makoto: Prof., Research Institute for Humanityand Nature
OKI Riko: Senior Researcher, Earth Observation Research Center, Japan Aerospace Exploration Agency

Research Program

Development of remote sensing technology for atmosphere and ocean observations

The Okinawa Subtropical Environment Remote-Sensing Center, an observation facility in Okinawa, Japan, was established by the National Institute of Information and Communication Technology (NICT). These facilities offer the use of full polarimetric Doppler radar (COBRA), 400 MHz wind profiler radar, Doppler sodar, disdrometers, rain gauges, and ocean radars. In 2005, an interuniversity collaboration was formed between NICT, Okinawa, and the Hydrospheric Atmospheric Research Center at Nagoya University, Japan (HyARC). Based on the results of collaboration studies, this fiscal year, the project has re-started with a new title as "Development of remote sensing technology for atmosphere and ocean observations" recognizing the demand of new techniques for the atmosphere and ocean remote sensing.

The Japan Aerospace Exploration Agency (JAXA) has developed a new dual Ka-band radar system for ground validation of the Global Precipitation Measuring Mission (GPM). As one of the atmosphere observations, rain observation experiment with this radar was conducted in NICT Okinawa with collaboration of JAXA. For the ocean observation, a new idea of flexible ocean radar idea has emerged. NICT performed basic development and the system seems very feasible. The new radar may be used for the Tsushima Current observation.

Research on Coast Circulation, Biological Production and Material Transport with Remote Sensing

Coastal area is between land and open ocean, and high biological production, active circulation and material transport are maintained by freshwater input with materials from land, including human origin, and by physical variations affected by topography. Because it is difficult to access to oceanic area, unlike on land, observation by remote sensing is very important. However, satellite sensors covering and resolving typical time and spatial scales in coastal area are limited, and remote sensing of coastal area is not fully operational because many technical problems still remain.

Scientists in Hydrospheric-Atmospheric Research Center have conducted research on development of remote sensing data and analysis of the data in coastal area, such as development of verification system of primary production, estimation and behavior of chlorophyll and suspended maters in East China Sea, red tide in Japanese coastal area, circulation in the East China Sea using sea surface topography and HF radar data. Japan Aerospace Exploration Agency (JAXA) is proposing new ocean color and sea surface topography sensors, and it is expecting that activities of remote sensing user community for coastal environment will be expanded.

Thus, a new research program, “Research on Coast Circulation, Biological Production and Material Transport with Remote Sensing”, has been started from 2011, and four collaborative research programs were accepted for following research topics.

-Developments of ocean color and sea surface height algorithms and verification around Japan and coastal areas.

-Application research on circulation of coastal area, biological production and material transport with those remote sensing data and combinations with other data and models

-Enhancement of international collaboration with Asian counties, specifically with Korea

8th Korea-Japan Workshop on Ocean Color Remote Sensing was also held in Korea Ocean Research and Development Institute as a part of the research program.

Advanced utilization of the polarimetric radars and the cloud-resolving model for cloud and precipitation research

Advanced research of cloud and precipitation with utilizing the polarimetric radars and the cloud-resolving model

The research program is aiming at a research frontier of cloud and precipitation physics by advanced utilization of various polarimetric radar parameters and the cloud-resolving model. In this year, three principal investigators (PIs) performed the following researches in the research program.

1. PI: Nakakita, E. (Kyoto University) To study formation and development of heavy rainfall, they performed the Okinawa Baiu observation in May and June and cumulonimbus cloud observation in Kobe area from September. These observations were combined with other observations such as the video sonde, millimeter-wave radar, and GPS to make various studies on cloud-microphysics processes.

2. PI: Wakazuki, Y. (University of Tsukuba) Since he develops a simplified data assimilation technique, he studied kinematic properties of convective clouds to contribute the technique development. In particular, a scheme to convert radar data to an idealized convective cell was developed. This enables us to relate the idealized convective cells derived from real rainfall distribution to convective cells produced by the cloud-resolving model CReSS.

3. PI: Sano, T. (Nagoya University) The purpose of the study is to clarify the heavy rainfall formation process in a basin and surrounding mountains in a warm season. Using the X-band polarimetric radar, precipitation systems in the Kofu basin and the surrounding mountains were studied. On July 28, 2010, a cumulonimbus cloud which was maintained for 6 hours above Asagiri plateau to the west of Mt. Fuji was observed. They revealed the maintaining process of the cloud and the formation process of heavy rainfall on the basis of the behavior of convective cells within the cloud.

Land-climate interaction through water and material cycles

Study on nonlinear and dynamic equilibrium interaction between land (i.e., vegetation, soil, topography) and climate through water cycle and material cycle need a new interdisciplinary approach including hydrology, forest science and ecology, in addition to climatology and meteorology. Based on results and issues from these different fields, this research plan aims to clarify how the land-climate interaction maintain and fluctuate and furthermore how the interaction relate the maintenance and variation of a whole climate system of the earth, focusing on water cycle. The main target area is the Asian monsoon region that includes the Eurasian Continent and the maritime continent with a complex topography and biodiversity.

On August 22 – 24, 2011, an international workshop on Asian monsoon and water cycle, co-hosted by MAHASRI, was held in Nhatrang, Vietnam. In this workshop about 80 participants attended from Japan, China, Taiwan, Malaysia, Vietnam, Philippines, Thailand and USA. Fifty participants presented new scientific results and there was a lively discussion. On November 15, a domestic workshop on climate-land interaction over Eurasia/ Asian monsoon region was held in HyARC, Nagoya University. Twelve participants gave interesting talks. Future issues on the land-climate interaction were also discussed.

The Innovative Program of Climate Change Projection for the 21st Century (KAKUSHIN Program)

●Cloud Modeling and Typhoon Research

The cloud modeling team has been developing a cloud-resolving model named the Cloud Resolving Storm Simulator (CReSS). The cloud microphysics and computation scheme of CReSS are improved for accurate and high-speed calculation. Convective clouds in the tropical region and typhoons are important objectives of our team. The CReSS model is also coupled with global models to simulate convective regions. CReSS is used for typhoon research with aims to help verify typhoon simulations made by global models and to produce accurate and quantitative evaluations of typhoon effects on human society under the current and warming climates. The program is ended in March 2012. Some of important results are summarized as follows.

●Improvement of the cloud-resolving model and typhoon simulations

Since typhoons are composed of intense convective clouds as well as associated stratiform clouds, a cloud-resoling model is necessary for accurate prediction of their intensity. In the present study, we have improved the CReSS model to perform simulation in an arbitrary-shaped computational domain. Using the cloud-resolving model, a simulation experiment with a computation domain along the typhoon track was performed. Figure 1 compares the simulation result of the typhoon No. 18 (2004) at 312 hours from the initial time (09 JST August 25, 2004) with the radar observation provided by JMA (the Japan Meteorological Agency). The position of the typhoon center, eye wall, surrounding spiral rainband and orographically enhanced heavy rainfall are correctly simulated. The result shows that the cloud-resolving model enables us to predict quantitatively the intensity of typhoon.

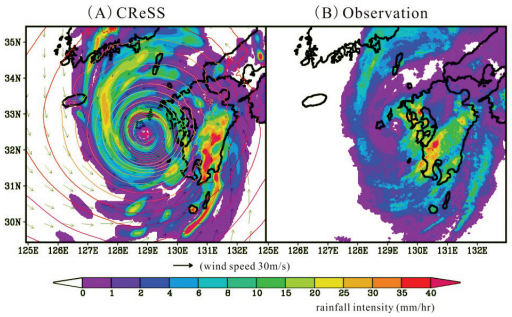

Fig. 1: (a) Simulation result of typhoon No.18 of 2004 using CReSS with the Tiling Domain Technique at 312 hours from the initial time (09 JST August 25, 2004). Color levels are rainfall intensity (mm hr^{-1}), contours are sea level pressure and arrows are horizontal velocity. (b) JMA radar observation at the same time of (a). Color levels are rainfall intensity (mm hr^{-1}).

●Projection of super-typhoons in global warming climate using the CReSS model

Observation, theory and numerical studies have been showing that intensity of hurricanes and typhoons increases with global warming. Since tropical cyclones such as typhoon bring a huge disaster in East Asia including Japan as well as water resources, future change of typhoon intensity with climate change will give a large impact on human society. In particular, intensity increase of the most intense category of typhoon is a big problem for disaster prevention planning and risk managements. Our team has studied maximum intensity of typhoons in the future (late-21 century) and near future (about 30 years later) climates in collaboration with the Extreme Event Projection team and found that some typhoons will become much more intense in the future climate that in the present-day climate. Typhoons with a surface maximum wind speed of 67 m s^{-1} or larger are referred to as “super-typhoon”. Number and intensity of super-typhoon will increase in the future climate. Moreover, super-typhoons will reach higher latitude such as the main islands of Japan because of higher sea surface temperature. Figure 2 shows a simulated super-typhoon by CReSS with a horizontal resolution of 2km. The super-typhoon moved northward over the Pacific and was making landfall over Japan with a central pressure of 880 hPa.

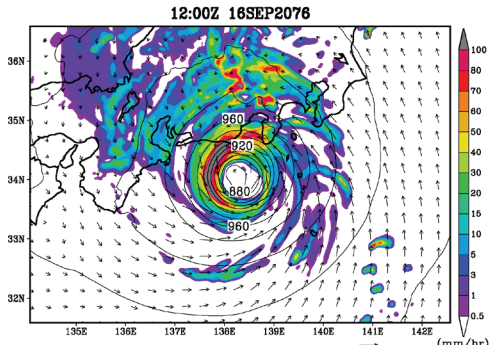

Fig. 2: The super-typhoon in the future climate (September 2076) simulated by the CReSS model. The contours are sea level pressure (hPa) and color levels are rainfall intensity (mm/hr).

Laboratory for Climate System Study

The modulation of the diurnal cycle of rainfall associated with the MJO observed by a dense hourly rain gauge network at Sarawak, Borneo

This study investigates temporospatial characteristics of the diurnal cycle (DC) of rainfall over Sarawak, western Borneo using a dense hourly rain gauge network. Their association with the large-scale intraseasonal disturbances is represented by the Madden-Julian Oscillation (MJO). The spatial pattern of the DC is divided between coastal and interior regions over the western part of Borneo, based on remarkable differences in rainfall peak times and amplitudes. The spatial distribution of daily rainfall in the active and break phases over Sarawak using the rain gauge datasets are shown in Fig. 1. In the active phase, rainfall over Sarawak increases relative to the break phase, although the spatial pattern of large rainfall amounts in the interior mountains and southwest coastal areas does not change greatly under either regime. The largest difference appears over the coastal region and foothills of the interior region. In particular, enhancement in rainfall is drastic near the coast. The spatial distribution of the rate of change in rainfall shows a clear difference. The coastal areas facing northwest show the largest change in rainfall from the break to active phase of MJO, whereas those facing north shows less change, and the mountain region in the interior of the island, where large amounts of rainfall occur, shows smaller changes still. Thus, the daily rainfall data derived from rain gauge increases in the active phase over the whole region, with coastal areas responding strongly to the MJO. And also, TRMM 3B42 rainfall is overestimated (underestimated) over the coastal (interior) regions compared with the rain gauge data. The TRMM shows that the rainfall between land and its surrounding oceans increases in the active phase. In surrounding ocean regions, the distribution of heavy rainfall areas extends to widely from the coastline to the open ocean in the active phase, are limited to near coastal areas in the break phase. It is found that the TRMM underestimates the impact of the MJO on rainfall compared with that estimated from the rain gauge data. However, the common message from both datasets is that the large-scale MJO influences rainfall differently over oceanic, coastal land and interior land areas, and does so consistently between the two datasets.

Although the amplitude of the DC and daily rainfall amount increase in the active MJO phase at all sites as shown in Fig.2, the MJO has a stronger effect in the coastal rather than the interior region. This modulation of rainfall in the interior region is dependant on an increasing frequency of rainfall. In the coastal regions, this is caused by the enhanced frequency and intensity of rainfall from the break to active phases of the MJO. Hence the change of the DC between the break and active phases in the interior region is explained by the change of the DC of frequency. On the other hand, the change of the DC in the coastal region is affected not only by the change of frequency but also by the intensity of rainfall. The DC in the coastal region is strongly affected by the characteristics of the oceanic DC, where the influence of the large-scale cloud system associated with the MJO is important.

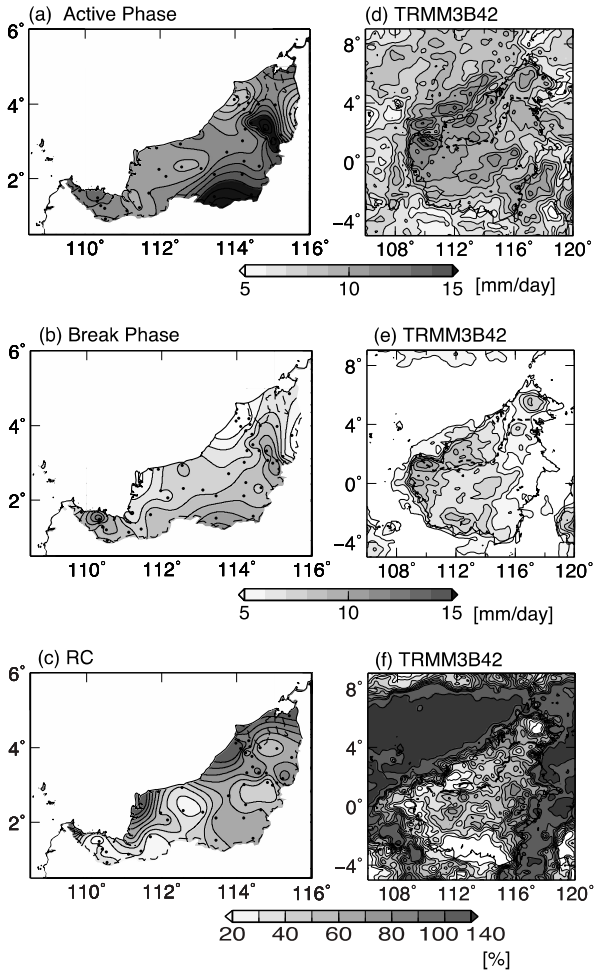

Fig. 1 : Composites of daily rainfall in (a) the active phase and (b) the break phase over Sarawak based on 50 rainfall stations. (c) Spatial distribution of rate (%) of change in rainfall from active phase to break phase, which is defined as [(active phase)/(break phase)-1] × 100. (d) to (f) Same as (a) to (c), but based on TRMM 3B42 data over Borneo and the surrounding ocean.

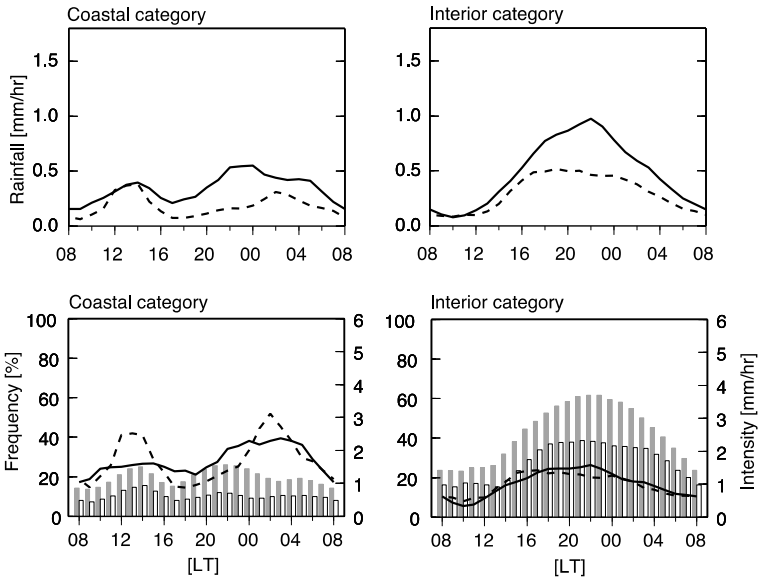

Fig. 2 : Composite of the DC of rainfall based on rain gauge in both the active phase and the break phase for coastal and interior categories (upper figures). The solid (dashed) line indicates the active (break) phase rainfall in the respective categories. Composite of the DC of frequency (%) and intensity (mm/hr) of rainfall for coastal and interior categories (bottom figures). The gray (white) bar indicates frequency of rainfall in the active (break) phase with right axis and the solid (dashed) line indicates intensity of rainfall in the active (break) phase with left and right axis, respectively.

Dominant modes of Trends and Interannual variations of summer precipitation in East Siberia

In Eastern Siberia, there exists great reaches of boreal forest, covering about14% of forests on the earth. This boreal forest play a great role in global hydrological and carbon cycles (eg., Zhang et al., 2011). It has been noticed that the growth of these boreal forests depends on interannual variability of summer precipitation. However, temporal and spatial variabilities of summer precipitation in Eastern Siberia has poorly been understood. In this study, we investigated dominant time-space patterns of interannual variability of summer precipitation in Eastern Siberia (90°E-140E,50°N-70°N), using the EOF (Empirical Orthogonal Function) analysis based upon daily precipitation grid data (APHRODITE, Yatagai et al.,,2011) from 1979 to 2007. The association of the EOFs of monthly precipitation with atmospheric circulation water vapor transport (and its divergence) fields are also analyzed, using the global objective reanalysis data from Japan Meteorological Agency (JMA).

We focused on the analysis of the top-three predominant patterns based on the contribution ratio of the EOFs. The first pattern (EOF1, contribution ratio: is 22.0%) represents the variation in the large area from central n to western region of Eastern Siberia (central Siberian highland) and combined with the southeast part of Eastern Siberia (far east Siberia) but with an opposite sign. The second pattern (EOF2, contribution ratio: is 13.8%) represents a dipole-like pattern (in precipitation variability) between east and west part of Eastern Siberia. The third pattern (EOF3, contribution ratio: is 9.3%) represents pattern of summer precipitation variability in northeast in Eastern Siberia.

These three EOF patterns have been proved to occur as a result of interaction between the westerly waves along 60 N with slight changes of trough (or ridge) system and water vapor field controlled by zonally-oriented stationary water vapor sources along 50-60N (possibly related to evapotranspiration from the boreal forest there) and by transport from the Arctic sea region.

In wet (dry) year in EOF1, deeper pressure trough (ridge) at around the Central Siberian Plateau (80E-120E) is likely to cause more (less) transport of water vapor from the Arctic sea (particularly from the Kara Sea). In wet (dry) year in EOF2, a pressure trough (ridge) at around western Central Siberian Plateau (80E) and a pressure ridge (trough) at around eastern Central Siberian Plateau (120E) is likely to cause more (less) water vapor transport from Laptev Sea (Arctic Sea) and less (more) transport from Kara Sea (Arctic sea). In wet (dry) year in EOF3, a pressure trough (ridge), remarkable only in a lower troposphere, extending from the Arctic Sea to Mongolia is likely to cause more (less) water vapor transport and convergence over regions of Verkhoyansk mountain Range and Mongolia. The time coefficients of the EOF1 show a remarkably increasing trend of precipitation in the Central Siberian Plateau region (Fig. 3a,b).

Finally, geographical pattern (or classification) for these interannual variation modes of precipitation has been deduced based upon the spatial eigen value patterns of the EOFs patterns as shown in Fig. 4: that is, the interannual variability of summer precipitation in western region of central Siberian plateau is relevant to EOF1 mode and that in Verkhoyansk Range on east bank of Lena River is relevant to EOF2 mode, and that in North Verkhoyansk Range is relevant to EOF3 mode.. It has also been found that the summer precipitation amount in central Siberian plateau has shown increasing trend particularly since 1990s.

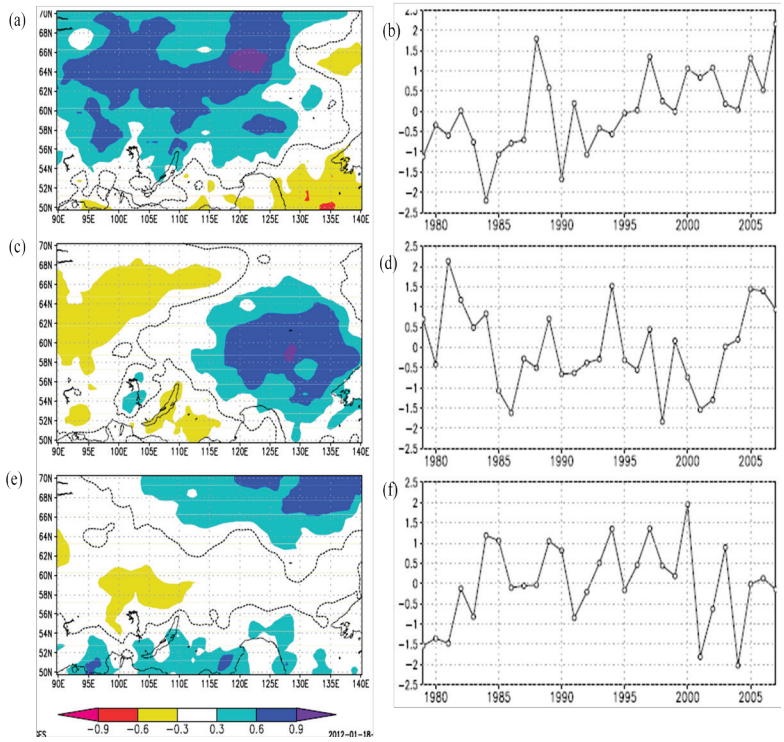

Fig. 3 : Spatial patterns and time scores (coefficients) of the three dominant three EOF modes in Eastern Siberia. (a), (b) for the EOF1, (c), (d) for the EOF2 and (e), (f) for the EOF3mode, respectively.

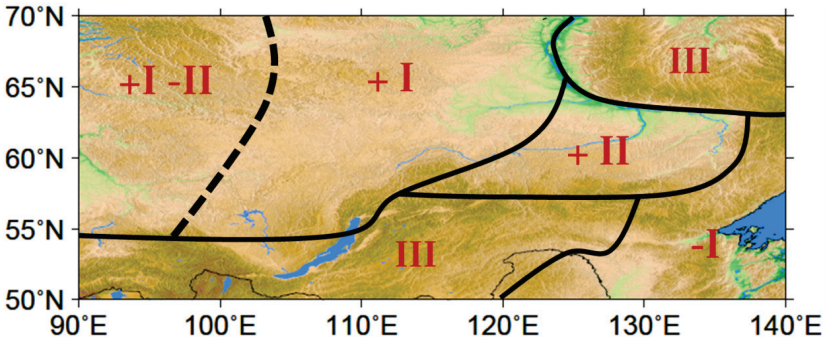

Fig. 4 : Regional patterns based on interannual variations of summer precipitation in Eastern Siberia. Regions I, II and III represent those for EOF1, EOF2, and EOF3, respectively. + or — represents variations with positive or negative sign for each time coefficients.

Laboratory for Cloud and Precipitation Climatology

On the Relationship between Tropical Precipitation and Tropospheric Humidity

The tropics, receiving significant rainfall more than a half as much as the global precipitation, is a key of global water cycle offering critical clues for understanding the mechanism driving the large-scale atmospheric circulation. Tropical atmospheres, however, are not tightly controlled by synoptic-scale dynamics such as baroclinic instability at work in mid latitudes, making it difficult to construct a comprehensive theory that explains the initiation and development of precipitation in the context of large-scale dynamics and thermodynamics. Controversies still remain despite of a long history of research to date on the environmental conditions governing the activation and suppression of tropical moist convection.

Observational evidence of the close relationship between mid-tropospheric humidity and precipitation has been found relatively recently and raised new research questions to address. Precipitation is known to increase exponentially with column relative humidity (CRH), but the rate of the increase disagrees among existing studies: compared to a satellite based daily climatology (Bretherton et al., 2004), the non-linearity of CRH as a function of precipitation turns out to be much stronger when constructed with in-situ measurements (Raymond et al., 2007). The current goal is to reconcile this apparent discrepancy.

The present work is, while based in either case on satellite data only, constituted of two different sets of analyses. The first utilizes daily mean climatology as done by (Bretherton et al., 2004), and the other applies the analysis method devised by Masunaga et al. (2012) to extract the variability on a time scale comparable to convective life cycles. This composite scheme is aimed at capturing the atmospheric variability over hourly to daily time scales in association with the development of convective systems as depicted in Figure 1.

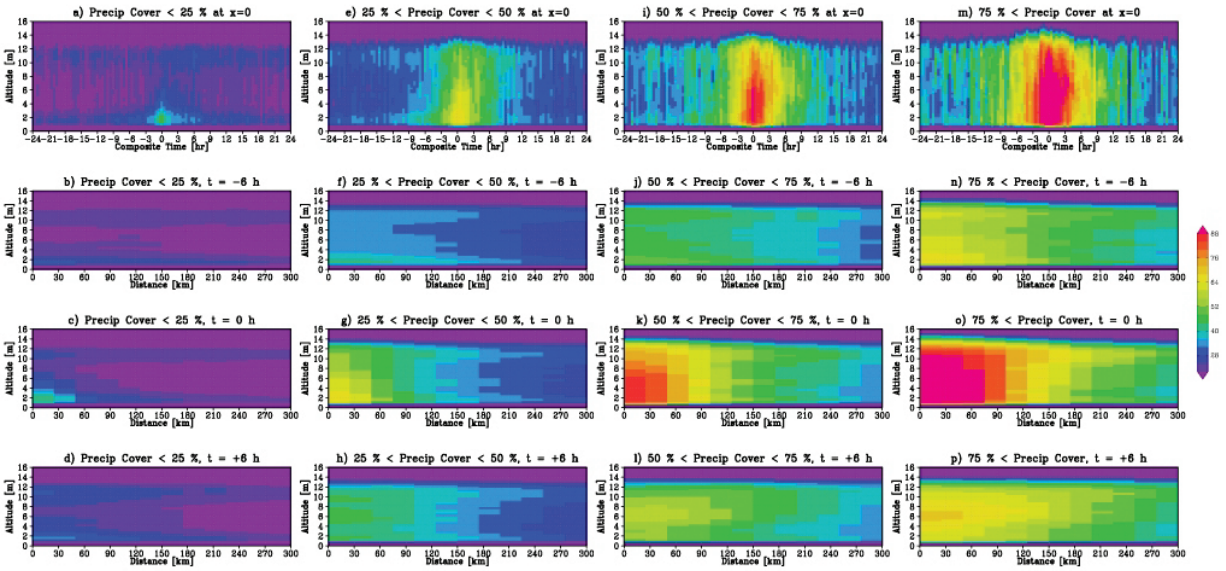

Fig. 1 : CloudSat cloud profiles composited against the TRMM detected convection. Time series (top) and vertically sliced snapshots at 6 hours before convection (upper-middle), at the time of convection (lower-middle), and 6 hours after convection (bottom). Composited separately for 4 types of convective systems from shallow cumulus (left) to very organized systems (right).

Figure 2 shows the observed relation between CRH and precipitation. It is evident that the non-linearity is much stronger when composited over a time scale of the convective life time (marked lines) compared to the daily climatology (solid line). The result implies that the known discrepancy arises from a difference in time scale of interest. The weak non-linearity in the daily climatology may be interpreted as a superposition of different types of convective systems combined together (Figure 3).

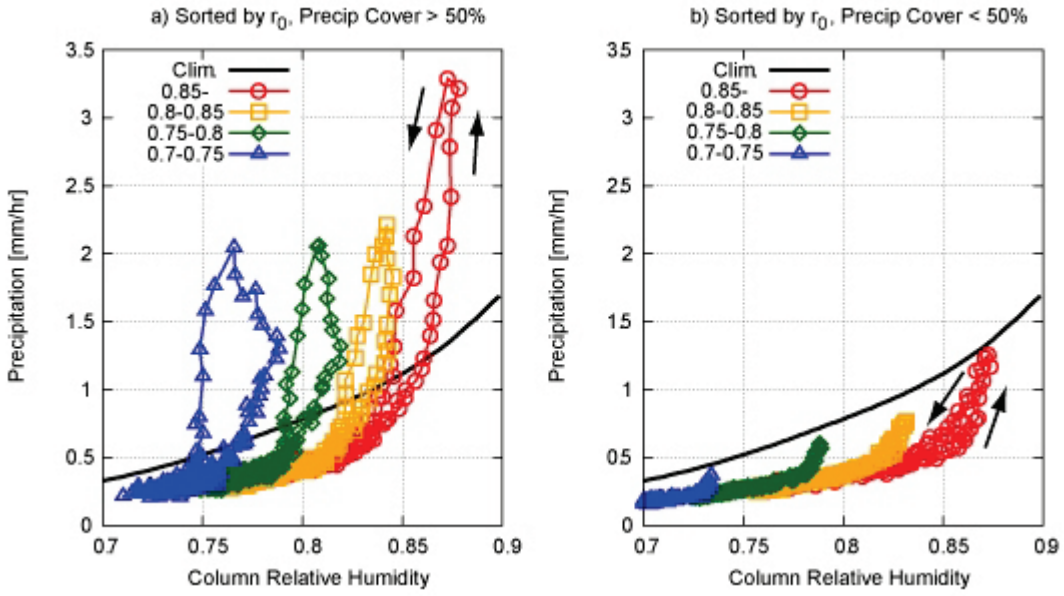

Fig. 2 : CRH-precipitation relationship from daily climatology (solid) and composite over a time scale of convective life cycles (marked) . Numbers in the legend refer to the CRH at the convective peak. Left) Organized convective systems (i.e., right half of Figure 1), Right) shallow convection (left half of Figure 1).

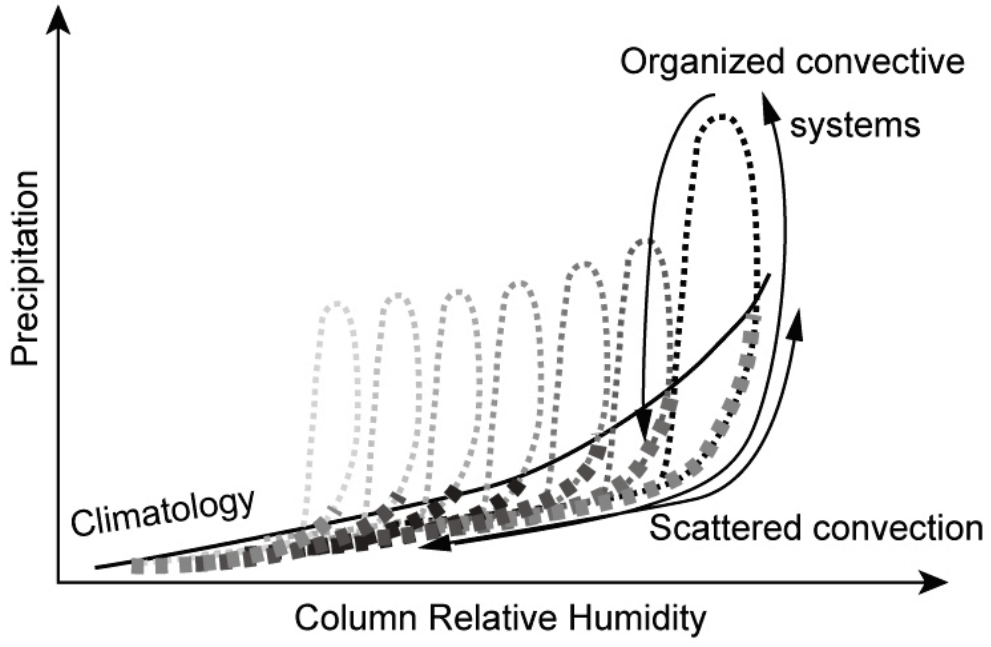

Fig. 3 : Schematic of the CRH-precipitation relation based on Figure 2.

Laboratory of Satellite Meteorology

Study on precipitation characteristics around Bangladesh using satellite data

It is well known that a rain activity is high not only during monsoon season but also during pre-monsoon season around Bangladesh, and the rain intensity is different between pre-monsoon season and monsoon season. In this study, the difference of precipitation systems with different rain intensities during pre-monsoon season and monsoon season are investigated using the long-term (13 yrs.) Tropical Rainfall Measuring Mission (TRMM) / Precipitation Radar (PR) data. It is clarified that there are also significant differences in these precipitation systems. The fraction of convective rainfall and rain top height are higher in pre-monsoon season than in monsoon season. The horizontal size of precipitation systems during pre-monsoon season is larger than monsoon season. The vertical structure of precipitation systems in pre-monsoon season are characterized by strong intensity up to high altitude and peak intensity at altitude of 3–3.5 km. On the other hand, the conditional rain-rate profile in monsoon season has no maximum and continues to increase from top to the lower part of the profile. Vertical variations of conditional rain-rate in monsoon season is smaller than in pre-monsoon season. Such differences of vertical structure of precipitation systems appear to be common in convective rainfall. Deep precipitation systems with intense rain dominate over the slope and foothills on the windward side of the Megalaya plateau, Chittagong hill tracts, and Himalaya mountains. Atmospheric fields associated with the difference of precipitaion systems around Bangladesh during two rainy periods are investigated using Japanese Re-Analysis 25 years (JRA25) data by classifying into rain cactive and break phases. As a result, the stability of the atmosphere seems to affect vertical profiles of the precipitation system. In the pre-monsoon season, mid-level air is very dry because of westerly wind from inland of India. During the active phase, air-layer has convective instability when warm and moist flow enters into the low-level over Bangladesh. Moreover, the air-layer with convective instability is raised by the orographic lifting over the Megalaya plateau, and convections are initiated. Then a deep system with intense rain is likely to be formed. On the other hand, during the break phase, atmospheric condition is unfavorable for rainfall development due to the incoming southwesterly moisture flow from the Bay of Bengal which is weaker than during the active phase. In the monsoon season, convective instability during the active phase is smaller than pre-monsoon season because the humidity at mid-level is high. Thus, moderate rainfall with low rain top height is dominant in monsoon season. During break phase, moisture amount from the Bay of Bengal seems similar during the active phase, but the incoming southeasterly moisture flow can easily escape from the flat lowland of northwestern Bangladesh into the Ganges Plain, and can cause a decrease in rainfall over Bangladesh.

Dual Ka-band Radar Experiment for GPM DPR Algorithm Development

A dual Ka-band radar system is developed by the Japan Aerospace Exploration Agency (JAXA) for the GPM DPR algorithm development. The dual Ka-radar system which consists of two identical Ka-band radars can measure both the specific attenuation and the equivalent radar reflectivity at Ka-band. Those parameters are important particularly for snow measurement. Using the dual Ka-radar system along with other instruments, such as a polarimetric precipitation radar, a windprofiler radar, ground-based rain measurement systems, the uncertainties of the parameters in the DPR algorithm can be reduced. The verification of improvement of rain retrieval with the DPR algorithm is also included as an objective.

Observations using the dual Ka-radar system were performed in Okinawa Island, in Tsukuba, over the slope of Mt. Fuji, and in Nagaoka, Japan. In Okinawa Island, the performance of the measurement has been confirmed by rain observation. In Tsukuba, one radar was directed in vertical and the other was in slant direction. By this configuration, total attenuation in the melting layer was estimated. The objective of the Mt. Fuji experiment was to observe the melting layer. An X band polarimetric radar was

simultaneously operated. Unfortunately, the melting layer did not come in between the two radars due to warm weather. In Nagaoka, a lot of wet snow fell, and much data on the snow have been obtained.

The main results are the k-Ze relationships. For the rain, reasonable k-Ze relationship has been obtained. The feasibility of total attenuation in melting layer has been studied. Different k-Ze relationships have been obtained in snow observations. Compared with rain, wet snow shows large specific attenuation. Figure 1 shows the concept of the vertical-slant path experiment and the radar echo examples. Using the difference in radar echoes due to the path length difference between vertical and slant paths, total attenuation in the melting layer can be estimated. Estimated attenuation in the melting layer was twice or three times larger of the ground-measured rain rates. The total attenuation seems to correspond to the estimates from the ground-based measurements

Fig. 1 : Concept of the vertical-slant path observation (left), and example of radar echoes (right).

Comparison of X-band multi-parameter radar network data

Operational test of X-band Multi-Parameter (MP) radar network installed by the River Bureau of the Ministry of Land, Infrastructure, Transport and Tourism, Japan (MLIT) has started from July 2010. By these radars, more detailed precipitation observation than the C-band radars of the Japan Meteorological Agency (JMA) is attained. On the other hand, TRMM (Tropical Rainfall Measuring Mission) is performing rain observation with precipitation radar (PR). In this study, comparison of the MP radar data installed in the Tokai area for nine cases from August 2010 to May 2011 is performed, and their rain rates are compared with TRMM PR and a disdrometer to clarify the characteristics of precipitation estimation of these three MP radars.

At first, each parameter (reflectivity (Zh), differential reflectivity (ZDR), specific differential phase (KDP) and rain rate (Rr)) is compared among three MP radars.

It turns out that all parameters except for KDP tend to underestimate depending on the distance from the radar. Vertical variation of rain seems to cause the underestimation.

KDP seems to be the most helpful to precipitation intensity estimation. However, when the rain rate (Rr) is compared with PR, the Rr derived from KDP is overestimated.

This overestimated value is about 1.3 times as large as Rr computed from a theoretical formula of the KDP-Rr relationship. Based on this result, Rr of MP radar is recalculated from KDP using the theoretical formula. And when comparing with PR, The obtained result becomes comparatively in agreement with PR (Fig.2). However, the differences appear in the case with local strong rains.

Finally, comparison of Rr computed from the theoretical formula with the disdrometer is performed.Rr computed from the KDP-R theoretical formula of MP radar is overestimated, while Rr computed from the Zh-R theoretical formula is underestimated.

Fig. 2 : Comparison of retrieved rain rate from TRMM precipitation radar and that of ground-based MP radar for the rain on 31 October, 2010.

Laboratory of Environmental Biophysics

Water use strategy of a Bornean tropical rainforest as a function of annual rainfall

Although Bornean tropical rainforests are among the moistest biomes in the world, they sporadically experience periods of water stress. The observations indicate that these ecosystems tend to have little regulation of water use, despite episodes of relatively severe drought (Fig. 1). This water-use behavior is often referred to as anisohydric behavior, as opposed to isohydric plants that regulate stomatal movement to prevent hydraulic failure. Although it is generally thought that anisohydric behavior is an adaptation to more drought-prone habitats, we show that anisohydric plants may also be more favored than isohydric plants under very moist environments where there is little risk of hydraulic failure.

To explore this subject, we examined the advantages of isohydric and anisohydric species as a function of the hydroclimatic environment using a stochastic model of soil moisture and carbon assimilation dynamics parameterized by field observations. The results showed that under very moist conditions, anisohydric species tend to have higher productivity than isohydric plants, despite the fact that the two plant types show almost the same drought-induced mortality. As precipitation decreases, the mortality of anisohydric plants drastically increases while that of isohydric plants remains relatively constant and low; in these conditions, isohydric plants surpass anisohydric plants in their productivity (Fig. 2).

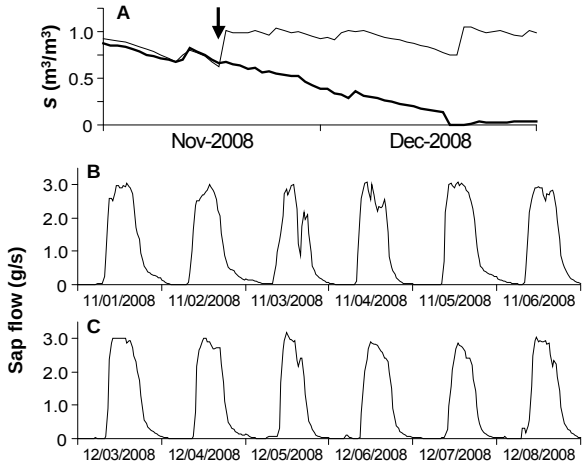

Fig. 1 : (A) Nomalized soil moisture content under the throughfall exclusion experiment (thick line) and normal (thin line) conditions., and sap flow rate of a Dipterocarpaceae tree (B) before and (C) after the experiment. Arrow means start of the experiment. There was little change in sap flow between normal and severe drought conditions.

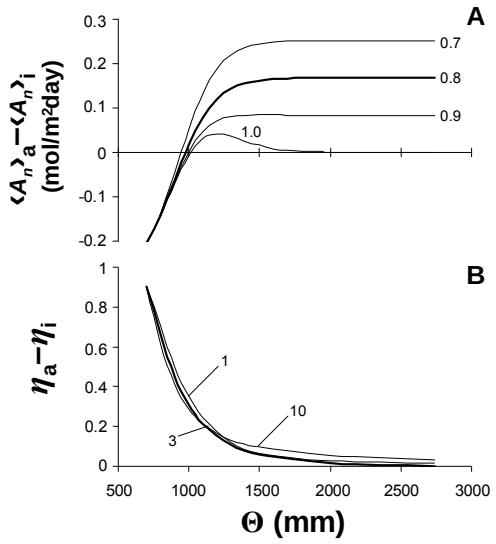

Fig. 2 : Differences in mean assimilation rate ($\langle A_n \rangle_a - \langle A_n \rangle_i$: A) and tree death index ($\eta_a - \eta_i$: B) between anisohydric and isohydric plants as functions of annual total rainfall (Θ) for a given frequency of rainfall events (λ = 0.54 day^{-1}). Lines represent different values of parameters for gas exchange characteristics (A) and tolerance against drought (B), as indicated by numbers alongside.

Drought-induced mortality of a Bornean tropical rainforest amplified by climate change

Drought-related tree mortality at a regional scale causes drastic shifts in carbon and water cycling in Southeast Asian tropical rainforests, where severe droughts are projected to occur more frequently, especially under El Niño conditions. We examine how the mortality of a Bornean tropical rainforest is altered by projected shifts in rainfall, using field measurements, global climate model (GCM) simulation outputs, and an index developed for drought-induced tree mortality (Tree Death Index η) associated with a stochastic ecohydrological model. All model parameters have clear physical meanings and were obtained by field observations.

Rainfall statistics as primary model forcing terms are constructed from long-term rainfall records for the late 20th century, and 14 GCM rainfall projections for the late 21st century. These statistics indicate that there were sporadic severe droughts corresponding with El Niño events, generally occurring in January–March, and that seasonality in rainfall will become more pronounced, e.g., dry (January–March) seasons becoming drier and wet (October–December) seasons becoming wetter. The computed η well reflects high tree mortality under severe drought during the 1997–1998 El Niño event. For the present, model results demonstrate high and low probabilities of mortality in January–March and October–December, respectively, and they predict that the difference in such probabilities will increase in the future. Such high probability of mortality in the dry season is still significantly high, even considering the beneficial effect of increased soil water storage in the wet season (which is projected to increase in the late 21st century) (Fig. 3).

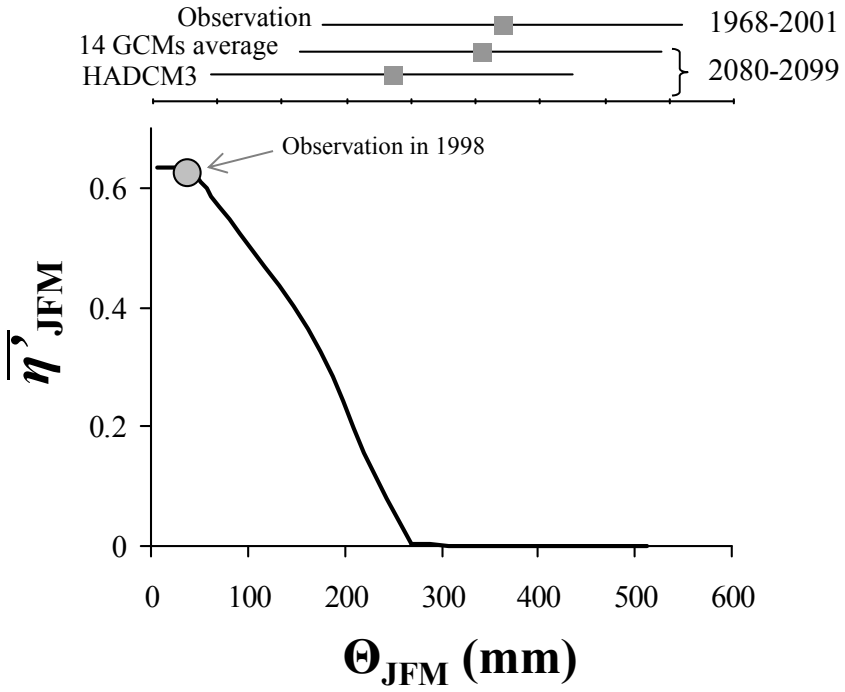

Fig. 3 : Mean total Tree Death Index in January-March (η'_{JFM}), considering effect of water storage in preceding October-December (s0) as a function of total seasonal rainfall in January-March (Θ_{JFM}). Also shown is η'_{JFM}, calculated using rainfall parameters obtained from observations under El Niño conditions in 1998. Upper part of the figure shows mean ΘJFM and standard deviations in late 20th century (observations from 1968-2001) and late 21st century (projections for 2080-2099 by the 14 GCM average and HADCM3).

Laboratory of Satellite Biological Oceanography

The susceptibility to photoinhibition of natural phytoplankton assemblages in the subarctic and subtropical gyres in the western north Pacific

Phytoplankton undergo a large change in irradiance due to the vertical transport by mixing (and turbulence) as well as the diurnal insolation cycle. Therefore, cells have evolved a variety of functions to acclimate oneself to the changing light fields, which resulted in taxonomic or inter-specific differences in the strategy for acquiring light energy. Such differences affect the competitive dominance among species under a given light condition. Species succession in nature is the key for ocean biogeochemical cycling because it can control a behavior of photosynthetically_produced materials via their morphological and chemical properties. Here we determined the physiological parameters on photoinhibition of natural assemblages in the subarctic and subtropical gyres in the western north Pacific to assess a regional difference in the light-acquiring strategy of dominant cells.

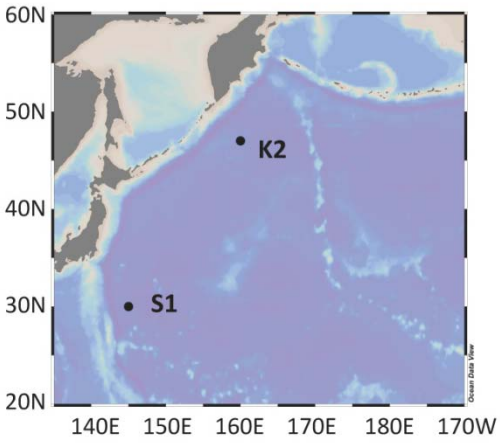

Fig. 1 : Sampling sites.

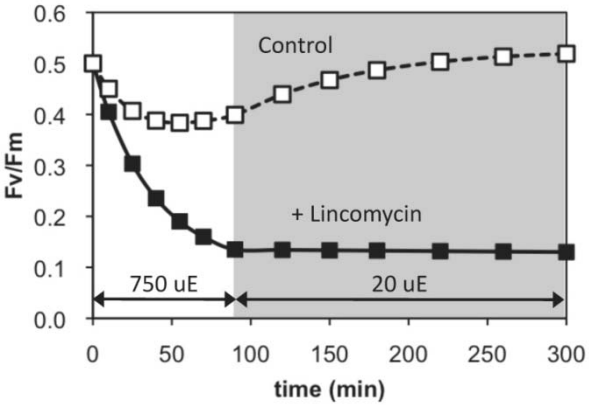

Fig. 2 : Maximum photochemical quantum yields of PSII (F_v/F_m) during the photoinhibition experiments for control (□) and lincomycin (absence of PSII repair: ■) treatments. Gray shaded areas depict low-light conditions of ~20 umol photons m^{-2} s^{-1} for 210 min, and white areas depict high-light exposure at 750 umol photons m^{-2} s^{-1} for 90 min. The difference between control and lincomycin treatments reflects PSII repair rate constants.

Photoinhibition experiments were conducted for phytoplankton in the surface waters of the station K2 (47°N, 160°E) and the waters from the surface and subsurface Chl maximal (SCM) layers of the station S1 (30°N, 145°E) during Feb. to Mar. (winter) and Jun. to Jul. (summer) in 2011 (Fig. 1). In the experiments, cells were exposed to high-light and the following low-light conditions, in which the maximum photochemical quantum yields of PSII (F_v/F_m) were monitored by using the fast repetition rate fluorometer (FRRF). Each sample was split into two bottles: one was supplemented with lincomycin to block chloroplast protein synthesis, thereby inhibiting PSII repair. Measurements of both treatments (with and without lincomycin) enable to estimate the susceptibility of PSII to photoinactivation (σ_i, $Å^2$ $photon^{-1}$) and the PSII repair rate constants (R_{PSII}, s^{-1}).

Regardless of season both parameters (σ_i and R_{PSII}) for cells in the surface waters exhibited higher values in S1 relative to K2 (Fig. 3a). This means that the subtropical phytoplankton were more susceptible to PSII photoinactivation while they recovered from high-light stress with more rapid PSII repair. Conversely, cells with less susceptibility to pthotodamage of PSII but less restorative capacity dominated in the subarctic conditions. This means that in K2 a lower-risk for pthotodamage would afford a competitive advantage since cells were exposed to wide (or rapid) changes in irradiance by deep (or active) mixing. Under ill-lit condition (~1% of the sea surface PAR) of the SCM layer of S1, dominant cells showed a remarkably lower ability of PSII repair relative to cells in the surface waters. Such less restorative capacity of cells found in the surface waters of K2 and the SCM layer of S1 may be attributed

to a lower light availability. In actual, after 2-days incubation under 25% or 3% of the surface PAR, cells in the SCM layer enhanced PSII restorative capacity in proportion to the light level (Fig. 3b). This implies that cells can acclimate to a light level by altering PSII repair rate within 2 days after the growth irradiance changes. In other words, it is essential for cells to grow that their risk of PSII photoinactivation is low enough to be compensated by the light-depended PSII repair rate. Then further understanding the mechanisms controlling σ_i of cells is needed in order to simulate the algal succession in the oceanic condition.

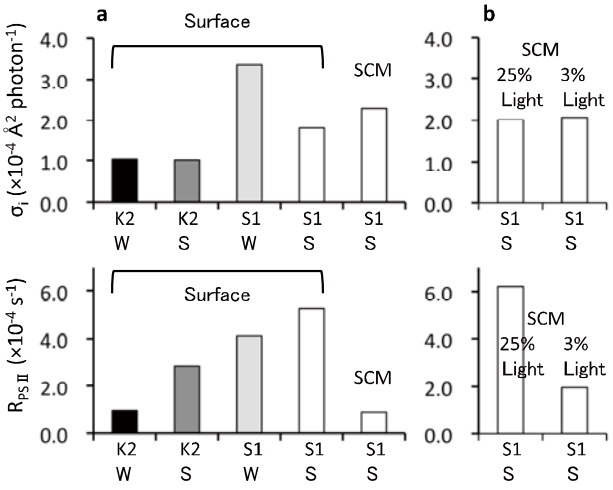

Fig. 3 : (a) Effective target size for photoinactivation of PSII (σ_i: upper panel) and PSII repair rate constants (R_{PSII}: lower panel) for cells collected in the stations K2 and S1.
(b) σ_i and R_{PSII} for cells in the SCM layer of S1 after 2-days incubations under two light levels (25% and 3% of the surface PAR).

Sinking processes of particulate matters in the center of the East China Sea

Large area of the East China Sea (ECS) occupied by a broad and shallow continental shelf surrounded by Japan, China and Korea. The spatial distribution of water mass of the ECS, especially during summer, is influenced by the discharge from the Changjiang. Accordingly, chemical and biological properties in the upper waters show heterogeneous distributions, mainly due to inputs of land-source and anthropogenic materials. The relatively high concentrations of satellite-derived chlorophyll (Chl) have been found to coincide with the distributions of less-saline, Changjiang Diluted Water (CDW; salinity <30 psu), which spreads eastward over the ECS during summer when the discharge increases. And east-west gradients of surface Chl (decreases with distance from the estuary) implies that nutrients derived by Changjiang are utilized by phytoplankton and gradually deplete. The decrease needs the processes that remove nitrogen and phosphorus from the CDW, but these remain unclear. Here, focusing on the sinking of particles as a removal process, we aim to assess the nitrogen budget in the water-column of the ECS and its relation to the CDW by using data of sediment trap experiments.

Two drifting sediment trap experiments were conducted in the ECS (around 31-32ºN, 125-126ºE) during the cruises of the T/V *Nagasaki Maru* in July 2010 and 2011. The sinking particles were captured at 10, 20, 30, 40m depths, and their mass and N contents were measured. During the experiments (3-5 days), both physical (temperature and salinity) and biogeochemical (Chl and nutrients) parameters were monitored in the study area by intensive CTD/water sampling casts. Concurrently, measurements of the primary productivity (from ^{13}C tracer bottle incubation), and sampling of suspended and sedimentary PN were also conducted. Vertical diffusion coefficients were estimated from observations using Turbulence Ocean Microstructures Acquisition Profiler (TurboMAP).

Figure 4a shows the nitrogen budget of the water column in the experimental area in 2010. The CDW was found covering the upper layer of 10 m depth, in which the concentration of dissolved inorganic nitrogen (DIN) was almost under the detection limit. Therefore, the productivity in the CDW was mainly supported by regenerated nitrogen. While, the amount of suspended PN in this layer was 46.6mmol_N, and 5% (2.1 mmol_N) of the PN sank below the depth of 10 m. In the layer of 10 to 20 m, there are pycnocline, nitracline, and subsurface Chl maximum (SCM; averaged Chl. conc.: 15 mg m^{-3}).

The upward flux of DIN by vertical diffusion at 20 m depth was estimated to be ~0.7 mmol_N m^{-2} d^{-1}, which corresponded to the magnitude of the sinking flux of PN from this layer (0.7 mmol_N m^{-2} d^{-1}). These results suggest that the diffusive DIN supply from below explained 15 % of nitrogen sources needed for productivity within the SCM layer (i.e. 85 % was supported by regenerated nitrogen). The ratio of PN flux at the 40 m (4.2 mmol_N m^{-2} d^{-1}) to the euphotic zone-integrated productivity (15.6 mmol_N m^{-2} d^{-1}) was 0.27, and a half was derived from the CDW.

In 2011, salinity of the upper water was relatively high, indicating less impact of Changjiang river water (figure 4b). Pycnocline, nitracline and SCM (averaged Chl. conc.: 2 mg m^{-3}) appeared at the relatively deeper layer (20 to 30 m). Correspondingly, magnitudes of productivity and sinking flux were one-third of those in the previous year. Through the base of nitracline around 30 m depth, both fluxes of DIN diffusion and PN sinking seemed to be balanced (= ~0.5 mmol_N m^{-2} d^{-1}), and this DIN diffusion supported 33% of the SCM productivity. Those results implied that a relative importance of new and regenerated nutrients for productivity of SCM layers would vary depending on the presence or absence of CDW.

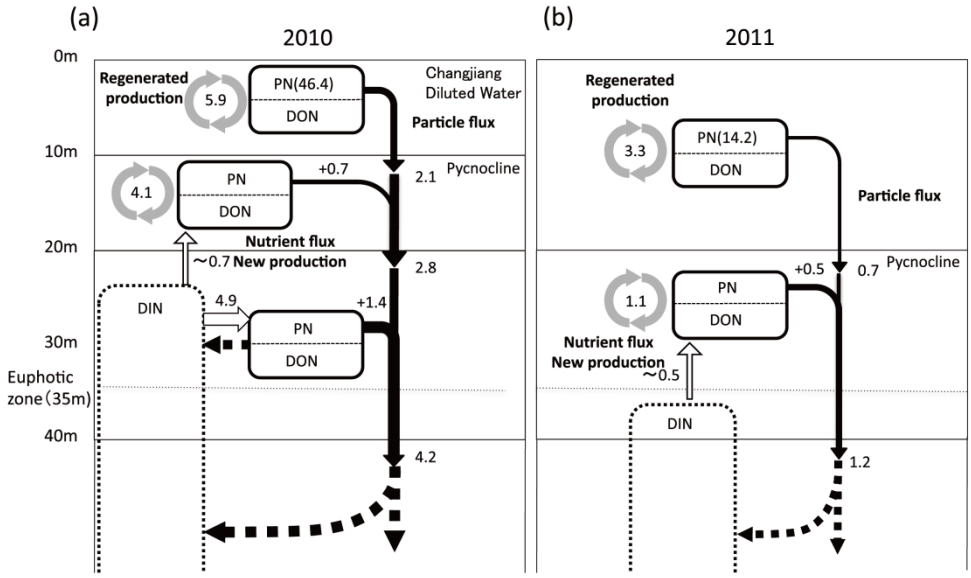

Fig. 4 : Nitrogen budget in the water column per unit area, and per day in trap experimental region in the East China Sea. Black, white and gray arrows show PN fluxes （mmolN m^{-2} d^{-1}）, DIN fluxes （mmolN m^{-2} d^{-1}） and depth-integrated primary productivity in each layer （mmolN d^{-1}）, respectively. Boxes with solid line and break line mean the suspended PN and dissolved organic nitrogen (DON) pools and the DIN pools. (a) 2010 and (b) 2011.

Inter-annual variation of giant jellyfish abundance and satellite observed phytoplankton bloom in the Yellow and East China Seas

Since 2002, massive appearances of *Nemopilema nomurai* were reported in northern East China Sea, Yellow Sea and the Sea of Japan almost every year, except 2008, 2010 and 2011. Source area of the larvae of jellyfish (ephyrae) was still unknown because the attached stages (polyp) of the jellyfish were never discovered in the field. Causes of jellyfish bloom were also not intensively explored, and it is required to study with environmental factors. Recently, new satellite datasets suring 1997 and 2010 with less influence of turbidity in the Yellow and East China Seas (Fig. 5, YECS) were produced from satellite ocean color sensors, SeaWiFS and MODIS/Aqua. Satellite derived time series of sea surface chlorophyll-a concentration (SSC), can be used as a proxy for phytoplankton biomass, and the data can be used to study the inter-annual variability. Phytoplankton blooms should stimulate the production of

zooplankton which, in turn, provides forage for larval jellyfish. Inter-annual variations of jellyfish abundance with the relation of these environmental variables were analyzed here based on the match/mismatch hypothesis.

Timing of phytoplankton bloom was derived fitting by Gaussian function;

$$Chl(t) = B_s\, x + B_i + a\, exp\left\{-\left[\frac{(x-t_p)^2}{2\sigma^2}\right]\right\} .$$

Chl(*t*) was SSC concentration, B_s was baseline slope, B_i was baseline intercept, a was peak concentration, t_p is peak time, t_p -2□ and t_p +2□ were defined as initiation and termination times of the bloom. Timing of phytoplankton blooms were compared with time of sea surface temperature (SST) become 15°C which is the temperature expected for separation of ephyrae from polyp.

At the mouth of Changjiang River (CRM), high SSC was observed during summer when SST became 15°C (Fig. 6). This is expected the influence of Changjiang River discharge. At the middle of Yellow Sea (YSM), spring bloom was observed March 20 - May 16, and it was before SST became 15°C. At Korean side of Yellow Sea (YSK), spring bloom was observed mostly March 20 - June 9, and SST became 15°C when bloom ended. At offshore of Changjiang River (CRO), spring bloom was observed mostly March 20 - June 1, and SST became 15°C during the bloom. Sporadic high SSC was observed after the spring bloom, and it was expected to be the influence of Changjiang Diluted Water. At China side of Yellow Sea (YSC), high (>1.5 mg m^{-3}) and low (< 1 mg m^{-3}) SSC occurred in winter and summer, respectively. SST became 15°C when the SSC became the minimum.

If SSC concentration can be used as an indicator of food for giant jellyfish ephyrae, CRM was most favorable condition for both timing and abundance. YSC and CRO may have been also good condition because of the sporadic higher SSC concentration but not as high as CRM. YSM and YSK should not be good condition because of the mis-match of spring bloom resulted low SSC concentration.

In all the areas, gradual increase of SSC was observed and indicating possible eutrophication of the areas, and, in this sense, food conditions for jellyfish may be becoming better. This may be one of reasons jellyfish bloom often occurred from 2002. SST was colder, timing to be 15°C was late in 2008, 2010 and 2011 than other years, and it may result no jellyfish bloom. However, the time difference of SST to be 15°C was not as large as variation of phytoplankton bloom timing. Thus, the hypothesis of match/mis-match of the phytoplankton bloom and ephylae may not explain the condition of recent non-jelly fish years.

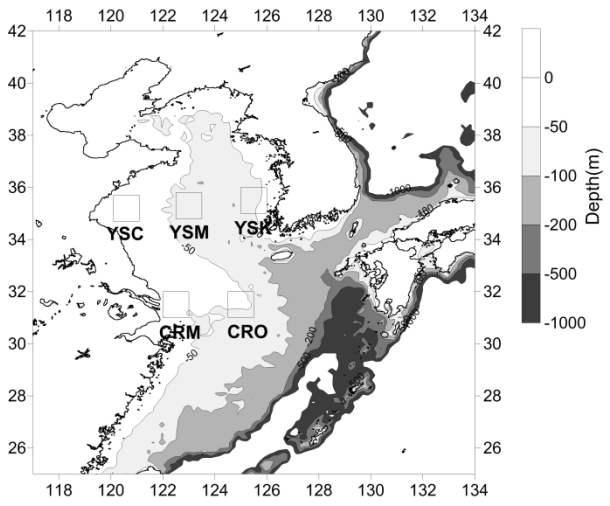

Fig.5 : Observation areas in the Yellow and East China Seas.

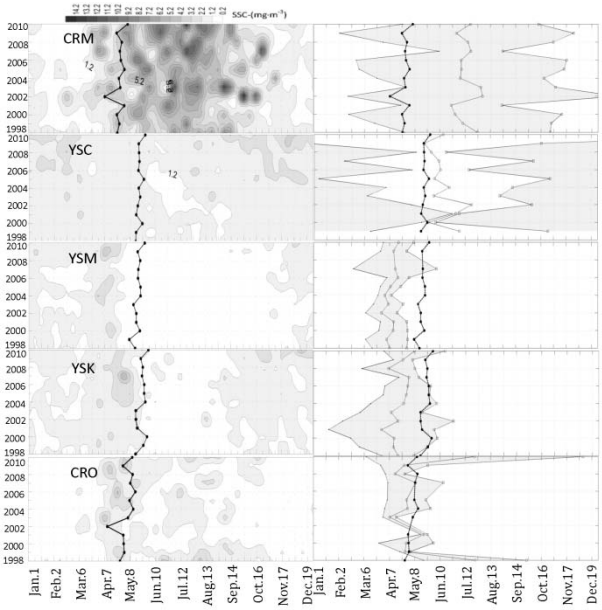

Fig.6 : SSC variations of weekly satellite data (left) and derived spring bloom timing (shaded area of right) in 1998-2010. Thick lines indicate time when SST became 15°C.

Loboratory of Bio-Physical Oceanography

Trajectory of giant jellyfish by satellite altimetry data.

Giant jellyfish blooming in the Japan Sea has damaged to fishery industry in recent years. The giant jellyfishes appear in the East China Sea and are transported to the Japan Sea by the current such as the Tsushima Warm Current. In the present study, we examined the possibility of trajectory of the giant jellyfish using satellite altimetry data. The particles regarded as giant jellyfish were tracked by Euler-Lagrange method. Initial condition of the calculation is applied from the distribution of visual observation result. Sea surface currents were derived every 7 days from sea surface current anomaly evaluated from satellite altimetry, climatological sea surface current calculated from a numerical model, and wind driven current estimated from sea surface wind data. The trajectory experiment was carried out the case in 2009, giant jellyfish blooming occurred and visual observations were conducted many times.

40 passive traces were set around Changjiang River mouth where giant jellyfish were observed on 10 June 2009 (Fig 1a) and were added every 72 minutes for 12 hours, and then 400 traces were tracked. The tracers deployed on 10 June were transported to the northeastward, and almost tracers distributed east of Cheju Island on 23 June (Fig. 1b). Since enormous giant jellyfishes were observed by visual observation, the result of tracer experiment was consistent with observation. Many of the tracers went through the Cheju Strait and then arrived in the western channel of the Tsushima Strait on 4 July. Giant jellyfishes were observed in the western channel of the Tsushima Strait on the same day by visual observation. It is suggested that giant jellyfishes observed in the Tsushima Strait on 4 July come from Changjiang River mouth taking about 1 month.

According to visual observation on 20 June, enormous giant jellyfishes distributed in the central part of the Yellow Sea. In order to investigate where the giant jellyfish were transported, tracer experiment was conducted. Almost tracers were transported to the northeastward and reach the west coast of Korea. This result suggests that giant jellyfish in the central part of the Yellow Sea were not transported to the Japan Sea.

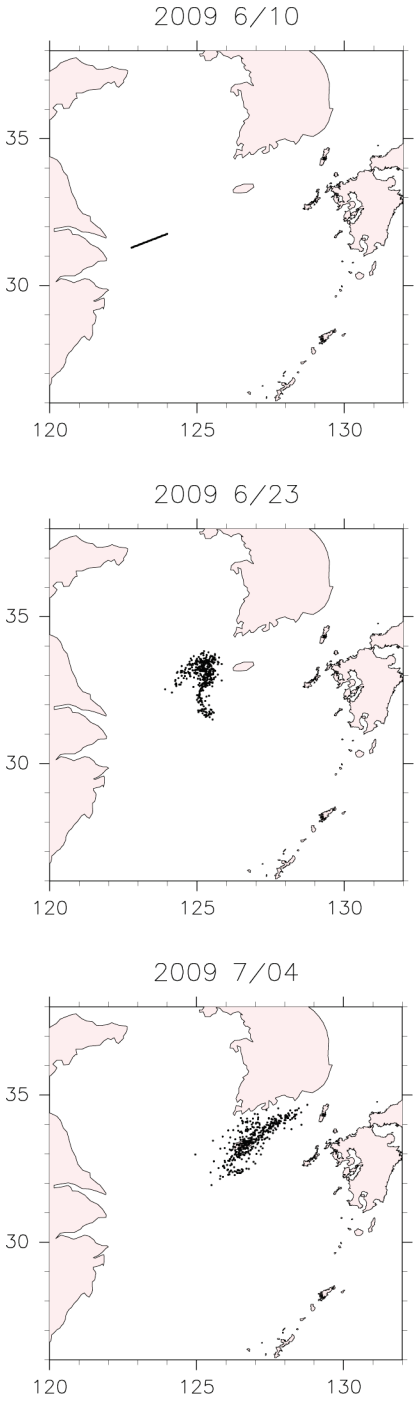

Fig.1 : Tracers distribution on (a) 10 June 2009 (b) 23 June 2009 (c) 4 July 2009.

Since visual observations were conducted only along ferryboat tracks, we carried out tracer experiment assuming the giant jellyfish distributed south of the ferry boat tracks. As a result, the tracers located south of 33°N were only transported to the Tsushima Strait.

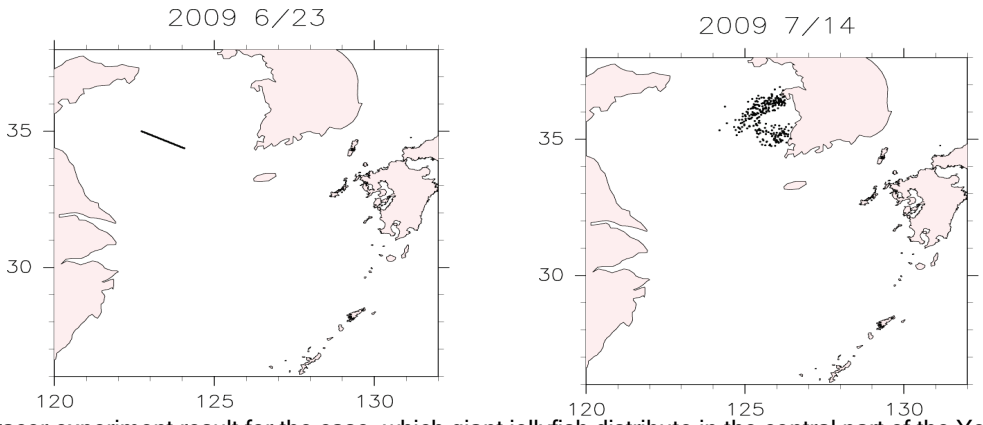

Fig. 2 : Tracer experiment result for the case, which giant jellyfish distribute in the central part of the Yellow Sea.

Interannual variation of the Tsushima Warm Current paths in the southwestern part of the Japan Sea

In order to examine the Tsushima Warm Current (TWC) paths, we created sea surface dynamical height (SSDH) and current field information data using Argos buoy trajectory and satellite altimetry data from May 1995 to October 2010. This data set has higher spatial-temporal resolution than that of ship observed data. We recognized that the TWC paths have not only seasonal variation but also interannual variation in the southwestern Japan Sea (SWJS).

To investigate the interannual variation in the TWC paths, the SSDH data were applied 13 months running mean filter. Empirical orthogonal function (EOF) analysis was applied to the low-pass filtered SSDH data to extract predominant mode. The first EOF mode indicated variation of the TWC paths along the east coast of Korea (Fig.1).

Since previous study suggested that the interannual variation in the TWC paths is synchronized with that of winter weather around Japan (Naganuma, 1985), we focused on the east Asian winter Monsoon Index (MOI) which indicates blowing of cold air into the Japan Sea. The interannual variation of MOI was created by applying three year running mean to remove shorter temporal variation (Fig. 2).

A cold-water upwelling occurs near the east coast of Korea in summer. Yun *et al.*(2004) reported that this cold-water originates from a water imposed cooling at the northwestern Japan Sea. Thus, we compared between latent/sensible heat flux in the northwestern Japan Sea and MOI, and correlation was significant. The correlation coefficient between temporal variation of the EOF first mode in summertime (June to August) and MOI was 0.66 which was more than 99% significant level (Fig.2). When MOI was low (1998) or high (2005), the TWC paths along the east coast of Korea taken different path. The results suggested that the TWC path along the east coast of Korea was varied with intensity of winter cooling.

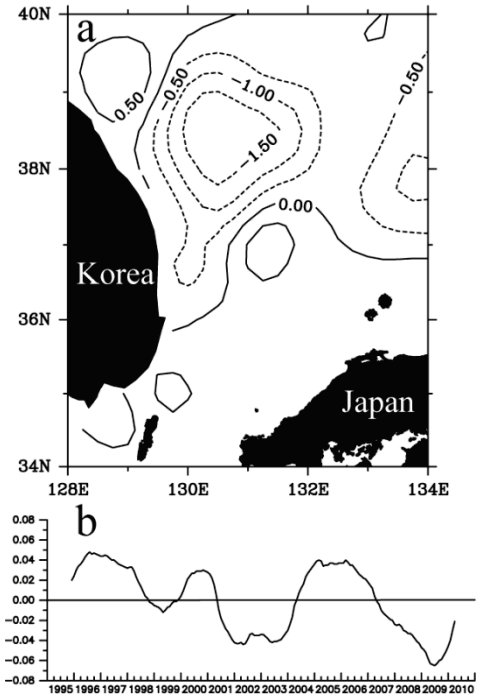

Fig. 1 : First EOF mode of the SSDH variability over the SWJS:
(a) spatial structure of first EOF,
(b) temporal variation of first EOF.
(Unit: m)

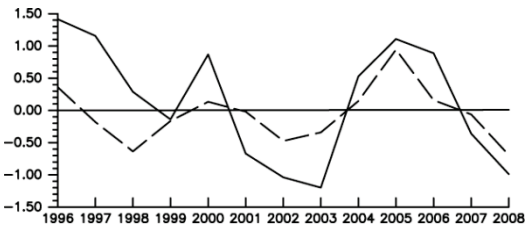

Fig. 2 : Normalized time series of summer time mean of temporal variation of first EOF (solid line) and MOI (broken line)

List of Publications

*:Staffs, students and research fellows in the HyARC.

1. Fujinami, H.*, D. Hatsuzuka, T. Yasunari*, T. Hayashi, T. Terao, F. Murata, M. Kiguchi, Y. Yamane, J. Matsumoto, M. N. Islam and A. Habib
   Characteristic intraseasonal oscillation of rainfall and its effect on interannual variability over Bangladesh during boreal summer. International Journal of Climatology, 31(8), 1192-1204, doi:10.1002/joc.2146, 2011.
2. Kim, H.-J., K. Takata, B. Wang, M. Watanabe, M. Kimoto, T. Yokohata and T. Yasunari*
   Global monsoon, El Niño, and their interannual linkage simulated by MIROC5 and the CMIP3 CGCMs. Journal of Climate, 24(21), 5604-5618, doi:10.1175/2011JCLI4132.1, 2011.
3. Kobayashi, N.* and T. Hiyama
   Stability Dependence of Canopy Flows over a Flat Larch Forest. Boundary-Layer Meteorology, 139(1), 97-120, doi:10.1007/s10546-010-9572-2, 2011.
4. Kume, T., N. Tanaka, K. Kuraji, H. Komatsu, N. Yoshifuji, T. M. Saitoh, M. Suzuki and T. Kumagai*
   Ten-year evapotranspiration estimates in a Bornean tropical rainforest. Agricultural and Forest Meteorology, 151(9), 1183-1192, doi:10.1016/j.agrformet.2011.04.005, 2011.
5. Masunaga, H.* and T. S. L' Ecuyer
   Equatorial asymmetry of the east Pacific ITCZ : observational constraints on the underlying processes. Journal of Climate, 24(6), 1784-1800, doi:10.1175/ 2010JCLI3854.1, 2011.
6. Miyazawa, Y., M. Tateishi, H. Komatsu, T. Kumagai* and K. Otsuki
   Are measurements from excised leaves suitable for modeling diurnal patterns of gas exchange of intact leaves? Hydrological Processes, 25(18), 2924-2930, doi:10.1002/hyp.8107, 2011.
7. Oka, E., T. Suga, C. Sukigara*, K. Toyama, K. Shimada and J. Yoshida
   “Eddy Resolving” observation of the North Pacific Subtropical Mode Water. Journal of Physical Oceanography, 41(4), 666-681, doi:10.1175/2011JPO4501.1, 2011.
8. Oue, M.*, H. Uyeda* and D.-I. Lee
   Raindrop size distribution parameters estimated from polarimetric radar variables in convective cells around Okinawa Island during the Baiu period. Asia-Pacific Journal of Atmospheric Sciences, 47(1), 33-44, doi:10.1007/s13143-011-1003-x, 2011.
9. Saba, V. S., M. A. M. Friedrichs, D. Antoine, R. A. Armstrong, I. Asanuma, M. J. Behrenfeld, A. M. Ciotti, M. Dowell, N. Hoepffner, K. J. W. Hyde, J. Ishizaka*, T. Kameda, J. Marra, F. Mélin, A. Morel, J. O'Reilly, M. Scardi, W. O. Smith Jr., T. J. Smyth, S. Tang, J. Uitz, K. Waters and T. K. Westberry
   An evaluation of ocean color model estimates of marine primary productivity in coastal and pelagic regions across the globe. Biogeosciences, 8(2), 489-503, doi:10.5194/ bg-8-489-2011, 2011.
10. Shiozaki, T., K. Furuya, H. Kurotori, T. Kodama, S. Takeda, T. Endoh, Y. Yoshikawa, J. Ishizaka* and T. Matsuno
    Imbalance between vertical nitrate flux and nitrate assimilation on a continental shelf : Implications of nitrification. Journal of Geophysical Research, 116, C10031, doi:10.1029/2010JC006934, 2011.
11. Siswanto, E., J. Tang, H. Yamaguchi, Y.-H. Ahn, J. Ishizaka*, S. Yoo, S.-W. Kim, Y. Kiyomoto, K. Yamada, C. Chiang and H. Kawamura
    Empirical ocean-color algorithms to retrieve chlorophyll-a, total suspended matter, and colored dissolved organic matter absorption coefficient in the Yellow and East China
    Seas. Journal of Oceanography, 67(5), 627-650, doi:10.1007/s10872-011-0062-z, 2011.

12. Son, Y. B., J. Ishizaka*, J.-C. Jeong, H.-C. Kim and T. Lee
Cochlodinium polykrikoides red tide detection in the South Sea of Korea using spectral classification of MODIS data. Ocean Science Journal, 46(4), 239-263, doi:10.1007/ s12601-011-0019-6, 2011.
13. Takikawa, T., G. Onitsuka, K. Fukudome, J.-H. Yoon, A. Morimoto*, M. Moku and A. Watanabe
Spatial and temporal variation of a cyclonic eddy detected downstream of the Tsushima Islands in November 2007. Estuaries and Coasts, 34(4), 775-784, doi:10.1007/s12237-011-9395-5, 2011.
14. Venkatraman, P.* and T. Yasunari*
Simulated changes in the atmospheric water balance over South Asia in the eight IPCC AR4 coupled climate models. Theoretical and Applied Climatology, 104(1-2), 139-158, doi:10.1007/s00704-010-0331-6, 2011.
15. Xu, J., K. Masuda, Y. Ishigooka, T. Kuwagata, S. Haginoya, T. Hayasaka and T. Yasunari*
Estimation and verification of daily surface shortwave flux over China. Journal of the Meteorological Society of Japan, 89A, 225-238, doi:10.2151/jmsj.2011-A14, 2011.
16. Xue, B.-L., T. Kumagai*, S. Iida, T. Nakai, K. Matsumoto, H. Komatsu, K. Otsuki and T. Ohta
Influences of canopy structure and physiological traits on flux partitioning between understory and overstory in an eastern Siberian boreal larch forest. Ecological Modelling, 222(8), 1479-1490, doi:10.1016/j.ecolmodel.2011.01.021, 2011.
17. Yamamoto, M., T. Ohigashi*, K. Tsuboki* and N. Hirose
Cloud-resolving simulation of heavy snowfalls in Japan for late December 2005 : application of ocean data assimilation to a snow disaster. Natural Hazards and Earth System Sciences, 11, 2555-2565, doi:10.5194/nhess-11-2555-2011, 2011.
18. Yamamoto, M. K. and K. Nakamura*
Typical patterns of microwave signatures and vertical profiles of precipitation in the midlatitudes from TRMM data. Journal of Applied Meteorology and Climatology, 50(6), 1236-1254, doi:10.1175/2010 JAMC2539.1, 2011.
19. Yamamoto, M. K., K. Ueno and K. Nakamura*
Comparison of satellite precipitation products with rain gauge data for the Khumb region, Nepal Himalayas. Journal of the Meteorological Society of Japan, 89(6), 597-610, doi:10.2151/jmsj.2011-601, 2011.
20. Yamashima, R., K. Takata, J. Matsumoto and T. Yasunari*
Numerical study of the impacts of land use/cover changes between 1700 and 1850 on the seasonal hydroclimate in monsoon Asia. Journal of the Meteorological Society of Japan, 89A, 291-298, doi:10.2151/jmsj.2011-A19, 2011.
21. Yasunari, T. J., A. Stohl, R. S. Hayano, J. F. Burkhart, S. Eckhardt and T. Yasunari*
Cesium-137 deposition and contamination of Japanese soils due to the Fukushima nuclear accident. Proceedings of the National Academy of Sciences, 108(49), 19530-19534, doi:10.1073/pnas.1112058108, 2011.
22. Zhang, N., T. Yasunari* and T. Ohta
Dynamics of the larch taiga-permafrost coupled system in Siberia under climate change. Environmental Research Letters, 6(2), doi:10.1088/1748-9326/6/2/024003, 2011.

Hydrospheric Atmospheric Research Center (HyARC)
Nagoya University

Furo-cho, Chikusa-ku, Nagoya 464-8601, Japan

Office:

Telephone: +81-52-789-3466

Facsimile: +81-52-789-3436

Home Page: http://www.hyarc.nagoya-u.ac.jp/Eng/index-en.html

The 2011 Annual Report was published July 2012 by the Hydrospheric Atmospheric Research Center (HyARC) Nagoya University.


HyARC
Hydrospheric Atmospheric Research Center, Nagoya University